Shape Gradient Computation in Isogeometric Analysis for Linear Elasticity

Louis Blanchard, Régis Duvigneau, Anh-Vu Vuong, Bernd Simeon

Shape Gradient Computation in Isogeometric Analysis for Linear Elasticity

Louis Blanchard, Régis Duvigneau, Anh-Vu Vuong, Bernd Simeon

Shape Gradient Computation in Isogeometric Analysis for Linear Elasticity

Louis Blanchard*, Régis Duvigneau*, Anh-Vu Vuong†, Bernd Simeon†

Project-Team Opale

Abstract: The transfer of geometrical data from CAD (Computer Aided Design) to FEA (Finite-Element Analysis) is a bottleneck of automated design optimization procedures, yielding a loss of accuracy and cumbersome software couplings. Isogeometric analysis methods propose a new paradigm that allows to overcome these difficulties by using a unique geometrical representation that yields a direct relationship between geometry and analysis. In this study, we investigate its use for sensitivity analysis and more specifically shape gradient computations, in the framework of linear elasticity problems. The potential of isogeometric analysis methods for shape gradient computations is demonstrated for two- and three-dimensional design problems.

Key-words: Shape derivative ; Isogeometric analysis ; Linear elasticity ; Structural shape optimization

* Opale Project-Team
† Technische Universität Kaiserslautern, Felix-Klein-Centre for Mathematics

Calcul de gradient de forme en analyse isogéométrique pour l'élasticité linéaire

Résumé : Le transfert de données géométriques depuis la CAO (Conception Assistée par Ordinateur) vers la simulation par éléments-finis est un goulot d'étranglement des procédures automatiques de conception optimale, conduisant à une perte de précision et à des couplages de codes pénibles. Les méthodes d'analyse isogéométrique proposent un nouveau paradigme, qui permet de surmonter ces difficultés en utilisant une unique représentation géométrique qui conduit à une relation directe entre la géométrie et la simulation. Dans cette étude, on explore son utilisation pour l'analyse de sensibilité et plus spécifiquement le calcul de gradient de forme, dans le cadre de problèmes en élasticité linéaire. Le potentiel des méthodes d'analyse isogéométrique pour le calcul du gradient de forme est démontrée pour des problèmes de conception bi- et tridimensionnels.

Mots-clés : Gradient de forme ; analyse isogéométrique ; Elasticité linaire ; optimisation de forme structurale

1 Introduction

This study concerns shape optimization problems for systems governed by PDEs (Partial Differential Equations) as encountered in engineering applications, e.g., in structural mechanics, fluid dynamics or electromagnetics. Multi-disciplinary optimization procedures are nowadays commonly used by engineers to solve complex problems in aeronautical or automotive industries, for instance. However, the processing of the geometrical data through the design loop is still a delicate issue: several different representations of the geometry coexist and several conversions are required, yielding additional overhead and extra difficulties from the theoretical and practical point of view.

Usually, the geometry of the engineering system of interest is defined using CAD (Computer Aided Design) software, on the basis of high-order representations. NURBS (Non-Uniform Rational B-Spline) basis functions are considered as standard in this context [15]. Cubic functions are often used, exhibiting a C^2 regularity.

The predominant analysis tools used to solve PDEs, such as FEA (Finite-Element Analysis) software, rely on a grid to describe the computational domain. The construction of this grid accounts for the geometrical data from CAD. However, a different representation is employed, since the grid usually defines the geometry with piecewise linear functions and C^0 regularity only. The task of generating the grid from CAD data is one of the most time-consuming in industry. Moreover, it is remarkable that some errors are introduced before any physical analysis has started.

Once the grid is available, the PDEs can be solved, and the resulting solution fields allow to estimate the performance of the current design. The optimizer can finally propose an update of the geometry in the CAD system to improve the performance. Here again, some inconsistencies occur, since the performance estimation is based on the approximate piecewise linear geometry, whereas the optimizer updates the high-order NURBS representation. The same inconsistencies hold for gradient estimates, if a gradient-based optimization method is employed.

The coexistence of these two geometrical representations makes the practical implementation of the design loop unnecessarily complex, since additional methods and software must be introduced: the automated update of the grid for any geometry change, the exchange of data between CAD and mesh generation tools as soon as automatic refinement is done on the boundary, the exchange of data between the solvers (multidisciplinary problems) as soon as the grid at the interface is modified, re-computation of the grid interface between different domains for problems with rotating elements, etc.

In the context of gradient-based optimization, the use of two geometrical representations makes also the estimation of the performance derivatives more complex, since the derivatives of the grid motion with respect to the NURBS parameters should be computed in the whole computational domain. This task may require to build the adjoint system of the mesh deformation method [12].

The isogeometric analysis approach, proposed recently by Hughes et. al. [3, 4, 11], promises to resolve or at least alleviate all these issues. It consists basically in solving PDEs with a variational approach on the basis of a NURBS representation originating directly from CAD. Thus, this approach promotes the integration of the two so far disjunct disciplines of FEA and CAD. Although this approach is especially beneficial for automated shape optimization procedures, as explained above, only a few studies can be found in the literature concerning its use for design problems [14, 16, 19]. Therefore, this study is devoted to the estimation of shape derivatives in this particular context. The concept of shape derivatives originates from Hadamard [10]. It has been studied from a theoretical point of view by several authors [7, 13, 17],

and also used to solve practical shape optimization problems (see for instance [1]).

In this study, we consider the framework of the linear elasticity equations, as outlined in Section 2. The application of isogeometric analysis to linear elasticity problems is described in Section 3 and validated on a typical problem in Section 4. Then, we introduce the concept of shape derivatives and its use in the isogeometric analysis context in Section 5. The resulting shape optimization procedure is described in Section 6 and validated in Section 7, for a problem with an analytical solution. Finally, a three-dimensional application is shown in Section 8 to demonstrate the capability of the proposed approach to tackle realistic problems.

2   Linear elasticity problem

We consider an open domain Ω in $d = 2$ or $d = 3$ dimensional space, which represents a deformable solid subject to external forces. Its boundary is composed of three disjoint parts, $\partial\Omega = \Gamma_N \cup \Gamma_D \cup \Gamma$ with $\Gamma \cap \Gamma_D = \varnothing$, $\Gamma \cap \Gamma_N = \varnothing$ and $\Gamma_N \cap \Gamma_D = \varnothing$. Dirichlet (imposed displacement) and Neumann (imposed stress) boundary conditions are prescribed on Γ_D and Γ_N, respectively, whereas Γ is considered as optimization variable (moving boundary). A zero Neumann boundary condition is prescribed on Γ.

The governing equations are the linear elasticity equations under the small deformation assumption. In case of zero body loads, the displacement field $\mathbf{u}$ is therefore the solution of the following system

$$\begin{cases} -div\,\sigma(\mathbf{u}) & = & 0 & \text{in}\,\Omega \\ \mathbf{u} & = & 0 & \text{on}\,\Gamma_D \\ \sigma(\mathbf{u})\cdot\mathbf{n} & = & \mathbf{g} & \text{on}\,\Gamma_N \\ \sigma(\mathbf{u})\cdot\mathbf{n} & = & 0 & \text{on}\,\Gamma \end{cases} \tag{1}$$

where $\mathbf{n}$ is the outward unit normal vector and $\sigma(\mathbf{u})$ the second-order stress tensor defined by Hooke's law

$$\sigma(\mathbf{u}) = 2\,\mu\,\epsilon(\mathbf{u}) + \lambda\,Tr\big(\epsilon(\mathbf{u})\big)\,Id. \tag{2}$$

Moreover, λ and μ are the Lamé parameters of the material and

$$\epsilon(\mathbf{u}) = \frac{1}{2}\left(\nabla\mathbf{u} + \nabla\mathbf{u}^T\right)$$

is the linearized strain tensor.

Like in the finite element method, the variational formulation of the linear elasticity problem defined by Eq. (1) is the starting point for isogeometric analysis. The weak form of (1) reads as follows: we seek for the physical displacement field $\mathbf{u} \in \mathcal{V} = \left\{\varphi \in H^1(\Omega)^d,\ \varphi = 0\,\text{on}\,\Gamma_D\right\}$ such that

$$\int_\Omega \left[2\,\mu\,\epsilon(\mathbf{u}):\epsilon(\mathbf{v}) + \lambda\,div\mathbf{u}\,div\mathbf{v}\right]d\Omega =$$
$$\int_{\Gamma_N} \mathbf{g}\,.\,\mathbf{v}\,d\Gamma \quad \forall\mathbf{v} \in \mathcal{V}. \tag{3}$$

By projecting the solution $\mathbf{u}$ and the test functions $\mathbf{v}$ to a finite-dimensional subspace $\mathcal{V}_h$ of $\mathcal{V}$ we next construct a numerical approximation.

3   Isogeometric analysis

The governing equations described in the previous section can be easily solved by means of a classical FEA approach. A suitable discretization of the domain is usually constructed by

introducing a mesh Ω_h that approximates the geometrical domain Ω. As demonstrated by Hughes et al. [3, 4, 11], this geometrical approximation of the domain has several drawbacks. In a few words, the use of an approximate geometry introduces some errors that could be avoided, the construction of the mesh is time consuming, and the coupling between different scientific disciplines is made unnecessarily complex.

Isogeometric analysis [3, 4, 11] is aimed at a better integration of FEA and CAD methods by using a unique representation basis for the geometry and the discrete solution fields. Isogeometric analysis proposes to discretize the computational domain exactly by using a NURBS basis originating from CAD.

3.1 NURBS representation

NURBS basis functions are defined in a parametric domain Ω_0. They can be represented in the physical domain Ω by introducing the transformation

$$F : \Omega_0 \to \Omega, \quad F(\boldsymbol{\xi}) = \mathbf{x}(\boldsymbol{\xi}). \tag{4}$$

Thus, any point of coordinates $\mathbf{x} = (x, y)^T$ in the physical domain Ω is mapped to a point of parameters $\boldsymbol{\xi} = (\xi, \eta)^T$ in the parametric domain Ω_0, as illustrated by Fig. 1. For the sake of simplicity, only the two-dimensional case is described here, but the extension to the three-dimensional case is straightforward.
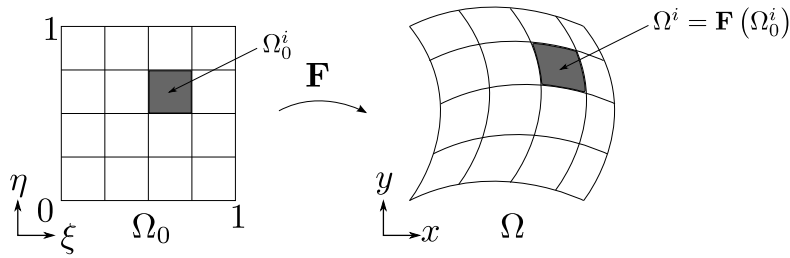

Figure 1: Mapping of the parametric domain Ω_0 to the physical domain $\Omega = F(\Omega_0)$.

Two- or three-dimensional NURBS basis functions are defined as the bivariate or trivariate tensor product of one-dimensional basis functions. The latter have compact support and are constructed using the so-called *knot* vector $\Xi = (\xi_0, \ldots, \xi_l) \in \mathbb{R}^l$ with $l = n + p + 1$, which consists of nondecreasing real numbers. Here, p is the degree of the functions and n the number of functions considered. Open knot vectors, i.e., knot vectors with first and last knots of multiplicity $p + 1$, are typically used [6, 9]. NURBS basis functions are rational extensions of B-Spline basis functions $N_{i,p} \ i = 0, \cdots, n$ that are computed recursively as

$$N_{i,0}(\xi) = \begin{cases} 1 & \text{if } \xi_i \leq \xi < \xi_{i+1} \\ 0 & \text{otherwise} \end{cases} \tag{5}$$

$$\begin{aligned} N_{i,p}(\xi) = & \frac{\xi - \xi_i}{\xi_{i+p} - \xi_i} N_{i,p-1}(\xi) \\ & + \frac{\xi_{i+p+1} - \xi}{\xi_{i+p+1} - \xi_{i+1}} N_{i+1,p-1}(\xi). \end{aligned} \tag{6}$$

Note that the quotient $0/0$ is assumed to be zero.

One-dimensional NURBS basis functions of degree p are then given by

$$R_{i,p}(\xi) = \frac{w_i N_{i,p}(\xi)}{\sum_{j \in \mathcal{J}} w_j N_{j,p}(\xi)} \tag{7}$$

where $w_i \in \mathbb{R}$ is the weight associated to the ith function, and $\mathcal{J} = \{0, \ldots, n\}$.

Two-dimensional NURBS basis functions are constructed using a bivariate tensor product (we omit the degrees p_ξ and p_η for the sake of readability)

$$R_{k\ell}(\xi, \eta) = \frac{w_{k\ell} N_k(\xi) N_\ell(\eta)}{\sum_{i \in \mathcal{I}} \sum_{j \in \mathcal{J}} w_{ij} N_i(\xi) N_j(\eta)}. \tag{8}$$

This representation requires two knot vectors $\Xi_\xi = (\xi_0, \ldots, \xi_{l_1})$ and $\Xi_\eta = (\eta_0, \ldots, \eta_{l_2})$. The extension to three-dimensional basis functions is straightforward. More details on the properties of NURBS can be found in [6, 9].

The transformation of the parametric domain Ω_0 to the physical domain Ω in Eq. (4) is defined by associating a *control point* to each basis function

$$\mathbf{x}(\xi, \eta) = \sum_{i \in \mathcal{I}} \sum_{j \in \mathcal{J}} R_{ij}(\xi, \eta) \mathbf{X}_{ij}, \tag{9}$$

where $\mathbf{X}_{ij} \in \mathbb{R}^2$ represents the coordinates of the control point of indices (i, j) in the physical domain. Using such a representation, the domain Ω is described as a single NURBS *patch*. The shape of the domain Ω is thus defined by the position of these control points, the weights, the knot vectors and the degrees of the basis.

NURBS representations are nowadays considered as standard for geometric modeling in CAD tools [15]. Thus, we assume this representation as exact. Isogeometric analysis proposes to employ such a parametric representation to solve the governing equations, without approximating the domain by a piecewise linear grid.

3.2   Galerkin projection

In the isogeometric paradigm, the same representation is employed for both the geometry and the physical fields. Therefore, according to Eq. (9), the discretized displacement field $\mathbf{u}_h$ is constructed as linear combination of the NURBS that define the geometry, i.e.,

$$\mathbf{u}_h(\mathbf{x}) = \sum_{i \in \mathcal{I}} \sum_{j \in \mathcal{J}} R_{ij}(\boldsymbol{\xi}) \mathbf{U}_{ij} = \sum_{i \in \mathcal{I}} \sum_{j \in \mathcal{J}} \hat{R}_{ij}(\mathbf{x}) \mathbf{U}_{ij} \tag{10}$$

where we define the basis functions $\hat{R}_{ij}$ in the physical domain by

$$\hat{R}_{ij}(\mathbf{x}) = \hat{R}_{ij}(x, y) = \hat{R}_{ij} \circ F(\xi, \eta) = R_{ij}(\boldsymbol{\xi}). \tag{11}$$

Note that the unknowns $\mathbf{U}_{ij}$ in this representation are two-dimensional vectors and comparable to control points. In general, they do not stand for displacements in specific nodes, as in the finite element method. Due to the usage of open knot vectors, however, the bivariate NURBS are interpolatory on the boundary, and thus the zero boundary conditions $\mathbf{u} = 0$ on Γ_D are easily enforced by setting those coefficients $\mathbf{U}_{ij}$ to zero that belong to the corresponding knots on the boundary Γ_D.

Eliminating those basis functions that are required to enforce the zero boundary conditions and renumbering the remaining basis functions and unknowns from $\ell = 1$ to m, we can write the numerical approximation in a standard fashion as

$$\mathbf{u}_h(\mathbf{x}) = \sum_{\ell=1}^{m} \mathbf{N}_\ell(\mathbf{x}) U_\ell = \mathbf{N}(\mathbf{x})\mathbf{U} \tag{12}$$

where $\mathbf{U} \in \mathbb{R}^m$ contains the unknown displacement coefficients and each column $\mathbf{N}_\ell(\mathbf{x}) : \mathbb{R}^2 \to \mathbb{R}^2$ of the $2 \times m$ matrix $\mathbf{N}(\mathbf{x})$ the NURBS basis functions R_{ij}, split into the components for the x and y-directions. In this way, the finite-dimensional subspace for the Galerkin projection is given by

$$\mathcal{V}_h = \operatorname{span} \{\mathbf{N}_\ell, \ell = 1, \ldots, m\}. \tag{13}$$

Consequently, the restriction of the variational formulation (3) to $\mathcal{V}_h$ leads to a system of linear equations

$$\begin{aligned}
\mathbf{K}\,\mathbf{U} &= \mathbf{F}, \\
K_{ij} &= \int_\Omega \left[2\,\mu\,\epsilon(\mathbf{N}_i).\epsilon(\mathbf{N}_j) + \lambda\,div(\mathbf{N}_i)\,div(\mathbf{N}_j)\right] d\Omega, \\
F_\ell &= \int_{\Gamma_N} \mathbf{g}\,.\,\mathbf{N}_\ell\,d\Gamma.
\end{aligned} \tag{14}$$

Compared to standard finite elements, the $m \times m$ stiffness matrix $\mathbf{K}$ is less sparse in general, which is due to the larger support of the NURBS. The entries of the stiffness matrix and also those of the force vector $\mathbf{F} \in \mathbb{R}^m$ are computed by applying classical quadrature rules. Actually, this integration is performed in the parametric domain, in accordance with the evaluation process of the NURBS in (5-7). Since the basis functions are defined on each knot interval, these knot intervals are often considered as elements in the isogeometric analysis terminology. Therefore, the above integration is carried out as usually in an element-wise way.

For the solution of the linear system with symmetric positive definite stiffness matrix, various standard methods can be applied. As long as the dimension remains moderate, a sparse direct solver, such as the multi-frontal method implemented in the UMFPACK library[5], is a good choice. The reader will find more details on the implementation in [3]. Techniques for local refinement are discussed, e.g., in [8, 18].

4 Remarks on the convergence properties of isogeometric analysis

The variational framework of the finite element method applies also to isogeometric analysis. In particular, this means that the best approximation property

$$\|\mathbf{u} - \mathbf{u}_h\|_E \leq \|\mathbf{u} - \mathbf{v}\|_E \quad \forall \mathbf{v} \in \mathcal{V}_h$$

holds with respect to the energy norm

$$\|\mathbf{u}\|_E^2 := \int_\Omega \left[2\,\mu\,\epsilon(\mathbf{u}).\epsilon(\mathbf{u}) + \lambda\,div(\mathbf{u})\,div(\mathbf{u})\right] d\Omega,$$

which is equivalent to the semi-norm $|\mathbf{u}|_{H^1(\Omega)}$ in $H^1(\Omega)$. Moreover, the numerical approximation $\mathbf{u}_h$ approaches the energy norm of the exact solution from below,

$$\|\mathbf{u}_h\|_E \leq \|\mathbf{u}\|_E.$$

Note that the energy norm of the numerical solution is available for free since it can be computed from the quadratic form

$$\|\mathbf{u}_h\|_E^2 = \mathbf{U}^T \mathbf{K} \mathbf{U}.$$

When refining a discretization, it must hold

$$\|\mathbf{u}_{h_1}\|_E \leq \|\mathbf{u}_{h_2}\|_E$$

where h_1 stands for the coarse and h_2 for the refined mesh. This property is often used to cross-check the numerical solution from a practical point of view.

The theoretical convergence properties of isogeometric analysis are quite similar to those established for the finite element method. We outline here the results of [2], assuming an invertible geometry parametrization F that is at least of class C^0. Let Q denote the analogue of an element in parametric space, i.e., Q is the cartesian product of $d = 2$ (or $d = 3$) non-empty knot spans. The function F maps this rectangle to $K = F(Q)$, which defines an element in physical space, with possibly distorted shape. If the degree of the NURBS used for the geometry and the discretization is p, then it holds at the element level

$$|\mathbf{u} - \mathbf{u}_h|_{H^1(K)} \leq Ch^p \sum_{i=0}^{p+1} \|\nabla F\|_{L^\infty(\tilde{Q})}^{i-p-1} |\mathbf{u}|_{H^i(\tilde{K})}. \tag{15}$$

Here, C is a constant that depends on the geometry of Ω but not on the meshsize parameter h, which is directly related to the size of Q. Furthermore, $\tilde{Q}$ and $\tilde{K}$, respectively, denote the support extension of Q and K, which is the union of the supports of those basis functions that are non-zero over Q.

By summing up over all elements, convergence of order p can then be established with respect to the H^1-seminorm. We remark that this estimate requires bounds for the i-th order seminorm of the solution $\mathbf{u}$, unlike for finite elements. Also, the parametrization enters the error bound and thus has a clear effect on the quality of the solution. If we measure the error in the H^k-seminorm where $k > 1$ and if the smoothness of the parametrization is less than C^{k-1}, the global error estimate requires the concept of so-called bent Sobolev spaces that take the reduced smoothness of the parametrization along specific knot lines into account, see [2] for more details.

As an example we look at the infinite plate with a hole already introduced in [11]. The shape and the boundary conditions are illustrated in Fig. 2. Symmetry along the coordinate axes is used, and the exact traction is employed for the Neumann boundary conditions. The underlying geometry parameterization is C^1. The convergence plot for the first principle stress σ_x for different degrees is shown in Fig. 3 and turns out to be as predicted by Eq. (15): the convergence rate increases with the degree.

5   Shape gradient computation

5.1   Optimization problem

We consider as optimization problem the minimization of the compliance subject to a constant mass constraint. The cost function, denoted $J(\Omega)$, depends on the shape of the domain Ω and is defined as

$$J(\Omega) = \int_{\Gamma_N} \mathbf{g} \cdot \mathbf{u} \, d\Gamma. \tag{16}$$

Therefore, the constrained shape optimization problem reads

$$\min_{\Omega \in \mathcal{U}_{ad}} J(\Omega), \quad \mathcal{U}_{ad} = \left\{ \Omega \subset \mathbb{R}^d, \int_\Omega d\Omega = V_0 \right\} \tag{17}$$

exact traction

Ω

$E = 10^5$

$\nu = 0.3$

symmetry

exact traction

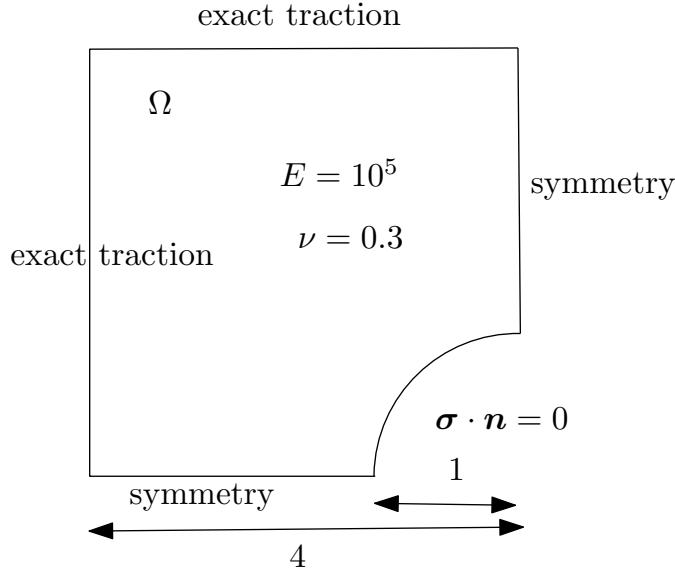$\boldsymbol{\sigma} \cdot \boldsymbol{n} = 0$

1

symmetry

4

Figure 2: Description of plate example

where $\mathcal{U}_{ad}$ is the set of admissible shapes and V_0 is the volume of the initial domain, considered as a reference volume. We refer to [7, 13, 17] to define precisely the conditions of existence and uniqueness of the solution for such a problem. To account for the constraint, we transform the problem defined in Eq. (17) into an unconstrained optimization problem using a Lagrangian formulation

$$\min_{\Omega \in \mathbb{R}^n} L(\Omega, \beta), \quad L(\Omega, \beta) = J(\Omega) + \beta \left(\int_\Omega d\Omega - V_0 \right) \tag{18}$$

where $\beta > 0$ is a positive Lagrange multiplier.

5.2 Shape derivative

In order to solve the problem in Eq. (18) using a gradient-based method, we introduce the concept of *shape derivative*. The theoretical foundations of this concept can be found in [7, 13, 17]. Let $\mathbf{v} : \mathbb{R}^d \rightarrow \mathbb{R}^d$ denote a sufficiently smooth admissible vector field that defines the shape deformation due to the optimization process. Let $T_t : \mathbb{R}^d \rightarrow \mathbb{R}^d$ denote the transformation which maps the initial domain Ω into the moving domain $\Omega_t = T_t(\mathbf{v})(\Omega) := \Omega + t\mathbf{v}(\Omega)$. Note that this deformation is different from the mechanical deformation of the system. The mapping introduced above is defined in physical space and is *a priori* independent of the mapping used in isogeometric analysis between the parametric domain Ω_0 and the initial physical domain Ω. However, as we will see later, the same NURBS basis functions will be used in practice, according to the isogeometric paradigm.

We describe next the main ingredients that allow to establish the expression of the shape derivative. Further details can be found in, e.g., [7]. Since the minimization of the compliance for a structural system governed by linear elasticity equations is self-adjoint, the computation of the shape derivative does not require the solution of an adjoint problem. By differentiating Eq. (16), under the assumptions that $\mathbf{g}, \mathbf{u} \in H^2(\Omega)$, it can be shown that the shape derivative
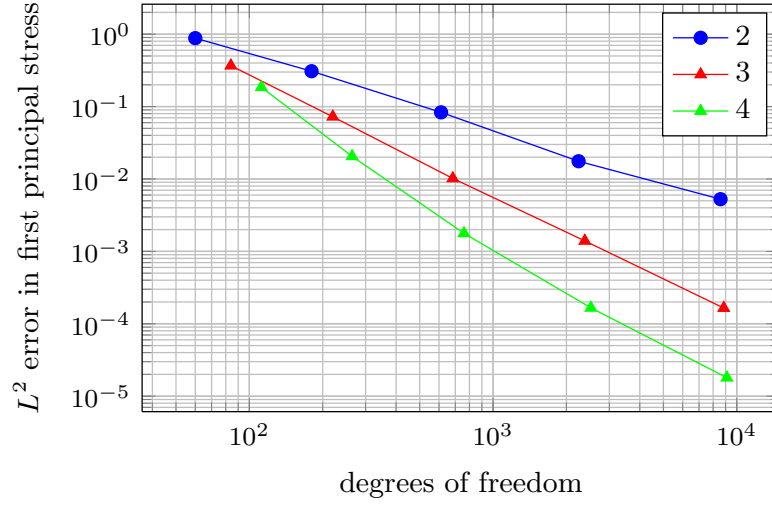
Figure 3: Convergence plot for the plate with a hole for different ansatz degrees

of the compliance for a given shape deformation $\mathbf{v}$ is

$$dJ(\Omega; V) = -\int_\Gamma \left(2\,\mu\,|\epsilon(\mathbf{u})|^2 + \lambda\,|div\mathbf{u}|^2 \right) \mathbf{v}.\mathbf{n}\,d\Gamma. \tag{19}$$

One can notice that the compliance can always be decreased by enlarging the domain: $\mathbf{v}.\mathbf{n} > 0$ implies that $dJ(\Omega; \mathbf{v}) \leq 0$. Similarly, the shape derivative of the Lagrangian function reads

$$dL(\Omega, \beta; V) = \int_\Gamma \left(\beta - \left(2\,\mu\,|\epsilon(\mathbf{u})|^2 + \lambda\,|div\mathbf{u}|^2 \right) \right) \mathbf{v}.\mathbf{n}\,d\Gamma. \tag{20}$$

Therefore, a possible choice to ensure a decreasing compliance is to consider a shape deformation $\mathbf{v}$ defined by

$$\mathbf{v} = \begin{cases} \left(2\,\mu\,|\epsilon(\mathbf{u})|^2 + \lambda\,|div\mathbf{u}|^2 - \beta \right) \mathbf{n} & \text{on} \quad \Gamma \\ 0 & \text{on} \quad \Gamma_D \cup \Gamma_N \end{cases} \tag{21}$$

where β is chosen to satisfy the constraint.

Eq. (21) defines the shape deformation of the boundaries $\partial\Omega = \Gamma \cup \Gamma_D \cup \Gamma_N$. However, it would be convenient to extend this definition on the whole domain Ω, in order to define the domain transformation T_t. From a practical point of view, this can be used to update the geometry as a whole. Consequently, we choose to extend the deformation field $\mathbf{v}$ using a linear elasticity model, which enables to re-use the structural elasticity solver. Finally, the deformation field is defined by solving

$$\begin{cases} -div(\sigma(\mathbf{v})) &= 0 & \text{in } \Omega \\ \mathbf{v} &= 0 & \text{on } \Gamma_D \cup \Gamma_N \\ \sigma(\mathbf{v}) \cdot \mathbf{n} &= (2\mu|\epsilon(\mathbf{u})|^2 + \lambda|div\mathbf{u}|^2 - \beta)\mathbf{n} & \text{on } \Gamma \end{cases} \tag{22}$$

One can notice that, in Eq. (22), we do not impose the deformation field v on the boundary Γ as a Dirichlet condition, but instead we consider a Neumann condition for $\mathbf{v}$. Actually, this choice is justified by two reasons. First, from numerical point of view, the deformation $\mathbf{v}$ will be defined using NURBS basis functions. Usually, the deformation defined by Eq. (21) does
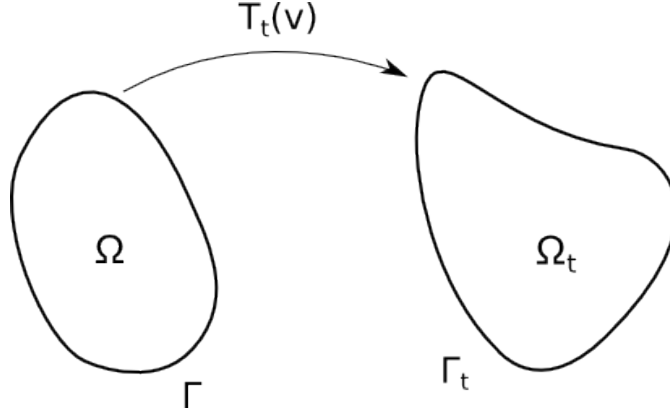
Figure 4: Mapping of the initial domain Ω to the moving domain $\Omega_t = T_t(\mathbf{v})(\Omega)$.

not belong to the NURBS space. Second, it is well known that the algorithms based on shape derivatives may suffer from a loss of regularity [7, 13, 17], that should be corrected by applying a smoothing operator. The use of such a Neumann boundary condition enables to increase the regularity of the deformation field $\mathbf{v}$.

Concluding, the problem defined by Eq. (22) is solved by using exactly the same approach as for the linear elasticity problem given by Eq. (1). In particular, an isogeometric approximation is employed, yielding a deformation of the domain in terms of control point displacements,

$$v(\mathbf{x}) = \sum_{\ell=1}^{m} \mathbf{N}_i(\mathbf{x}) V_i. \tag{23}$$

The components V_i that constitute the motion of the control points are thus obtained by solving a linear system similar to Eq. (14),

$$
\begin{aligned}
\mathbf{K}\,\mathbf{V} &= \mathbf{C}^1 - \beta\,\mathbf{C}^2, \\
\mathbf{C}_i^1 &= \int_\Gamma \left(2\,\mu\,|\epsilon(\mathbf{u})|^2 + \lambda\,|div\mathbf{u}|^2\right) \mathbf{N}_i\,.\,\mathbf{n}\; d\Gamma, \\
\mathbf{C}_i^2 &= \int_\Gamma \mathbf{N}_i\,.\,\mathbf{n}\; d\Gamma.
\end{aligned}
\tag{24}
$$

The stiffness matrix $\mathbf{K}$ is defined by equation (14), $\mathbf{V}$ is the vector of the deformation control points and $\mathbf{C}^1$, $\mathbf{C}^2$ are the external force vectors, which include the terms for the shape derivative and constant volume constraint. Actually, the system above is solved twice to compute $\mathbf{K}^{-1}\mathbf{C}^1$ and $\mathbf{K}^{-1}\mathbf{C}^2$. Then, for any Lagrange multiplier β, the deformation field $\mathbf{V}$ can be computed without extra cost by

$$\mathbf{V} = \mathbf{K}^{-1}\mathbf{C}^1 - \beta\,\mathbf{K}^{-1}\mathbf{C}^2. \tag{25}$$

6   Shape optimization algorithm

The shape optimization procedure used in the numerical experiments presented in the next sections can be summarized by the following algorithm:

1. Initialization of the domain defined by the control points $\mathbf{X}^0$ and counter $k = 0$

2. Start of optimization loop

3. Solve system (14) for the domain defined by the control points $\mathbf{X}^k$, yielding the structural displacement defined by the control points $\mathbf{U}^k$

4. Solve system (24) for the domain defined by the control points $\mathbf{X}^k$, yielding the shape deformation defined by the control points $\mathbf{V}^k$

5. Initialization of step length t^k

6. Start of the line search

7. Compute the Lagrange multiplier β^k such that the domain defined by the control points $\mathbf{X}^{k+1} = \mathbf{X}^k + t^k\mathbf{V}^k$ is admissible

8. Solve system (14) for the domain defined by the control points $\mathbf{X}^{k+1}$, yielding the structural displacement defined by the control points $\mathbf{U}^{k+1}$

9. Compute the compliance for the domain defined by the control points $\mathbf{X}^{k+1}$

10. If the compliance decreases then the step length t^k is retained, else t^k is reduced and goto (7)

11. End of line search

12. If converged then stop, else $k \leftarrow k + 1$ and goto (3)

13. End of optimization loop

We underline the fact that, according to the isogeometric analysis paradigm, a unique basis is used to represent the geometry of the domain, the structural displacement field and the deformation field for the optimization. Nevertheless, the hierarchical property of NURBS can be used to refine this representation if required. Typically, an accurate resolution of the elasticity equations requires the use of a refined representation. On the other hand, the shape optimization problem can be solved by using a few degrees of freedom.

7   Shape optimization validation

A two-dimensional test-case is first considered to validate the shape gradient computation and the optimization procedure. It deals with a classical shape optimization problem in linear elasticity, for which the solution is known analytically. We consider a square flat plate with a hole located at its center, subject to uniform external normal forces. The objective is to determine the complete shape that minimizes the compliance for a constant plate area. The initial shape of the moving boundary is defined by four straight lines. The configuration of this test-case is illustrated by Fig. 5. Only a quarter of the geometry is considered for symmetry reasons. Additional geometrical constraints are thus introduced to maintain the extremities of the moving boundary on the symmetry axes.

   We define the computational domain by a single bi-quadratic patch, which exhibits a singular point at the top left corner, as shown in Fig. 6. The 12×7 net of control points can be seen in this figure. Since quadratic basis functions are used, two superimposed control points permit to create the singularity at the top left corner. The optimization problem counts 24 variables that correspond to the coordinates of the 12 control points defining the moving boundary (in red in the figure). This test-case has already been studied using an isogeometric approach in [19], but without using the shape gradient concept.
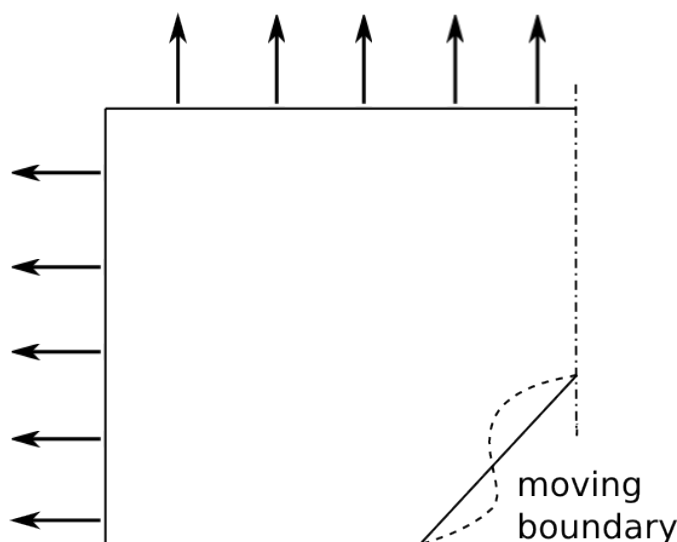
Figure 5: Description of the validation test-case.

   The shape gradient defined on the moving boundary is depicted in Fig. 7 for the initial domain and in Fig. 8 after 11 iterations. One can notice in particular the balance between the motion to reduce the compliance and the motion to maintain a constant area. As seen, the moving boundary shape evolves progressively towards a circle, which is the solution of the problem. The final domain is depicted in Fig. 9. As can be observed, the domain parameterization remains perfectly symmetric. One can notice a crossing of some control points in the vicinity of the hole. However, the parameterization remains injective which enables to solve the systems.

   The fast convergence of the optimization procedure is illustrated in Fig. 10. Convergence is achieved in about 20 iterations, with results that are very close to those presented in [19]. This shape optimization exercise allows to assess the shape gradient computation which steers the optimization procedure in the isogeometric context.
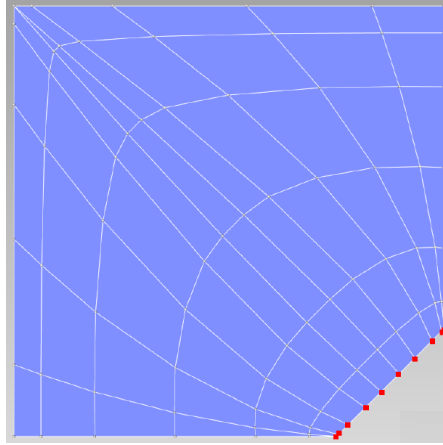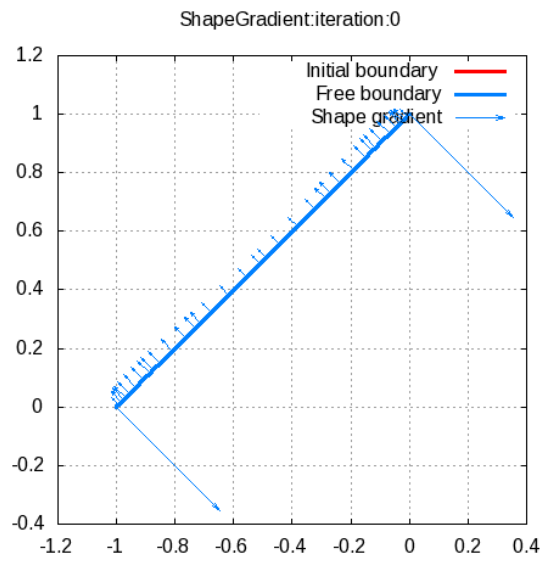
Figure 6: Initial domain.

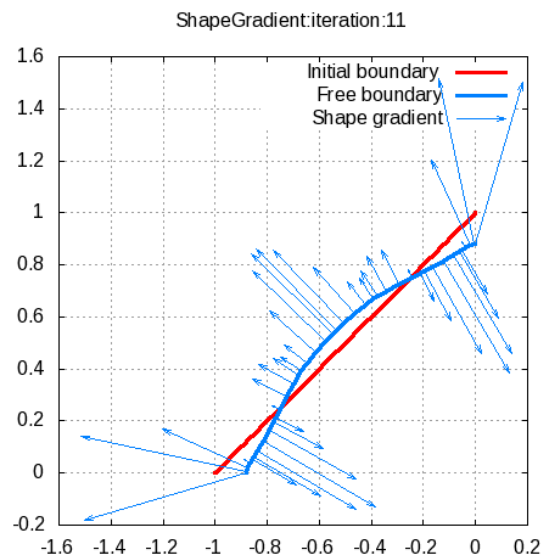Figure 7: Shape gradient for initial domain.

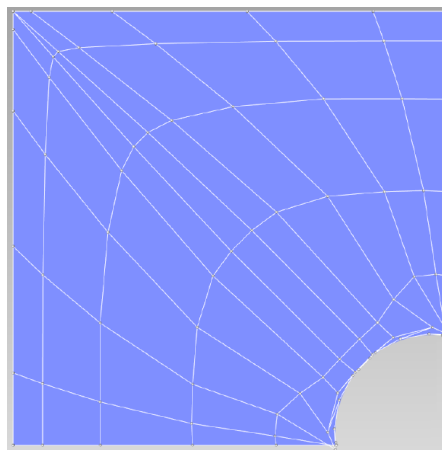Figure 8: Shape gradient at the11th iteration.
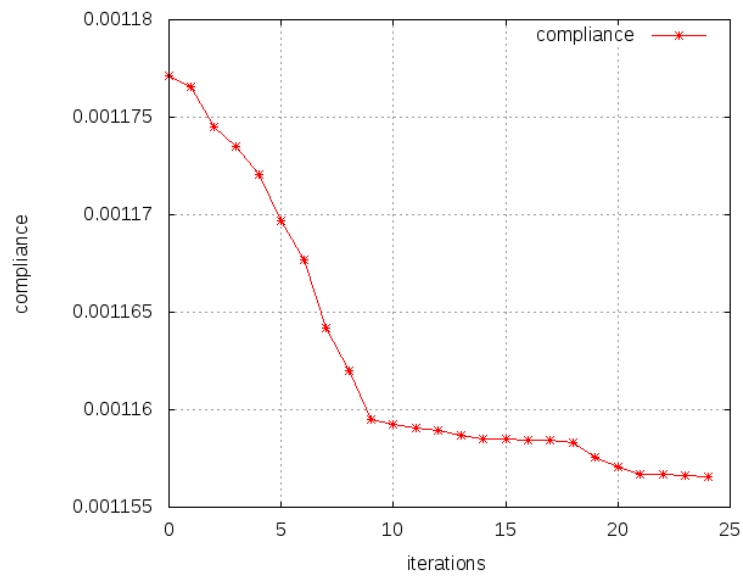

Figure 9: Final domain.

Figure 10: Evolution of cost function.

8 Application to 3D problems

The proposed methodology is finally applied to a three-dimensional design problem. The objective is to optimize the shape of an open-spanner, which is subject to Dirichlet conditions at one extremity (zero displacement) and Neumann conditions at the other extremity (imposed external forces), as illustrated by Fig. 11. The initial domain is depicted in Fig. 12. A similar two-dimensional problem has been proposed in [19]. For this three-dimensional extension, two problems are considered successively: in a first optimization exercise, only the top and bottom boundaries are considered as optimization variables, whereas in a second exercise the shapes of the lateral boundaries are also optimized. The objective is again the reduction of the compliance, subject to a constant volume constraint. Additional constraints are also imposed to maintain the shape of the open-spanner symmetric with respect to horizontal and vertical planes. Since the boundary conditions are non-symmetric, the computational domain represents the whole open-spanner, as shown in Fig. 12.
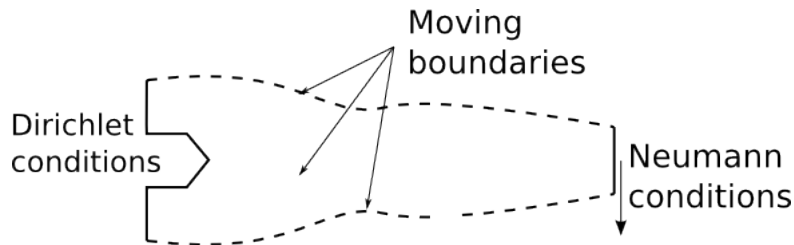
Figure 11: Description of the open-spanner test-case.
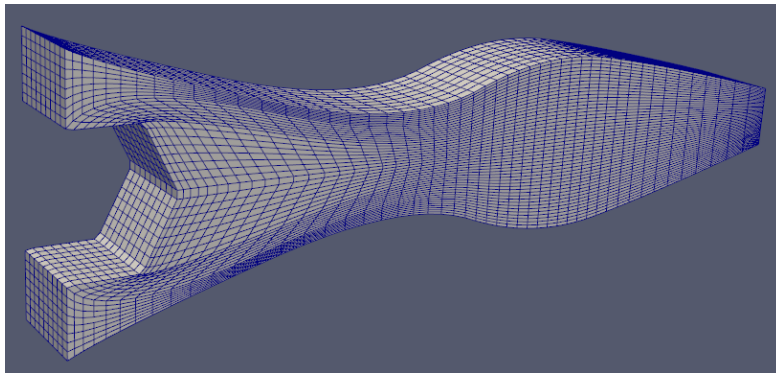

Figure 12: Initial domain.

The domain is parameterized using linear basis functions in the vertical and crosswise directions and quadratic functions in the lengthwise direction. The net of control points counts $6 \times 7 \times 2$ points in horizontal, vertical and crosswise directions, respectively, and is depicted in Fig. 13 for the initial domain. Thus, the two optimization exercises account for 48 variables (16 control points) and 192 variables (64 control points), respectively.

The evolution of the cost function during the optimization procedure is displayed in Fig. 14. Convergence is achieved in a few iterations and for a very low computational time. Obviously, a lower compliance value is reached for the second optimization exercise, which includes a larger number of variables. A comparison of initial and final domains is presented in Fig. 15 for the
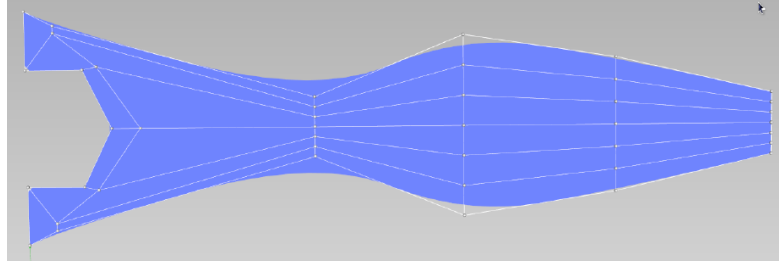
Figure 13: Initial domain parameterization.

first exercise and in Fig. 17 for the second one. The displacement fields are depicted in Fig. 16 and Fig. 18. The optimization procedure yields an enlargement of the left part of the open-spanner, whereas the right part becomes thinner to fulfill the constant volume constraint. For the first exercise, one can notice that the lateral boundaries are slightly modified, although they are not considered as optimization variables. This is due to the fact that the side boundaries are considered as Neumann conditions for the Eq. (22) that defines the shape evolution. The shape obtained is very close to that found in [19] for a two-dimensional problem. For the second exercise, the open-spanner is made thinner in the crosswise direction, which enables to enlarge it significantly. A closer look at the displacement fields shows that the maximum displacement value, at the right extremity, is significantly reduced during the optimization, especially in the second exercise.
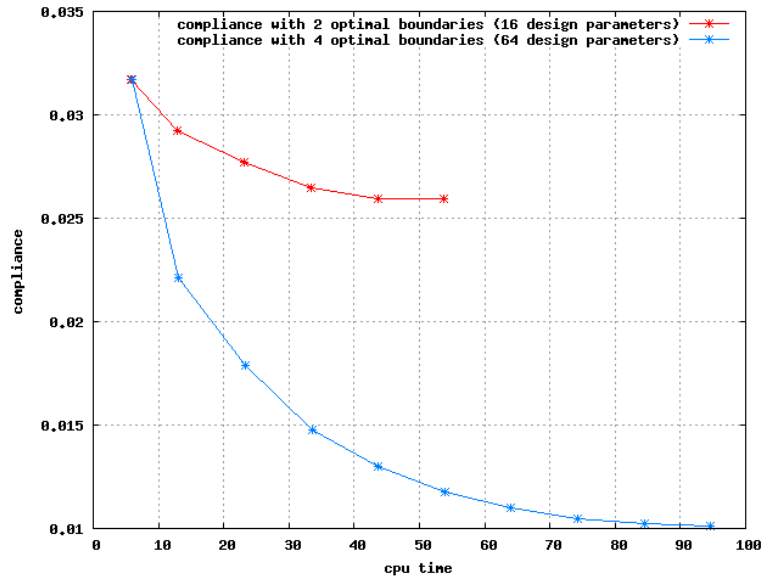

Figure 14: Cost function evolution for the two optimization exercises with respect to CPU time.
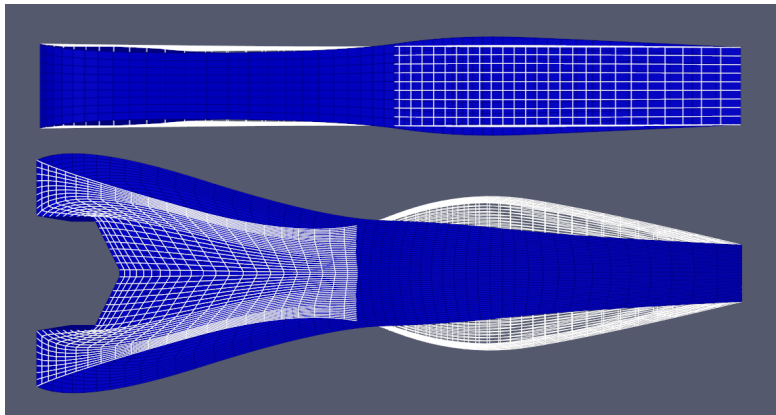
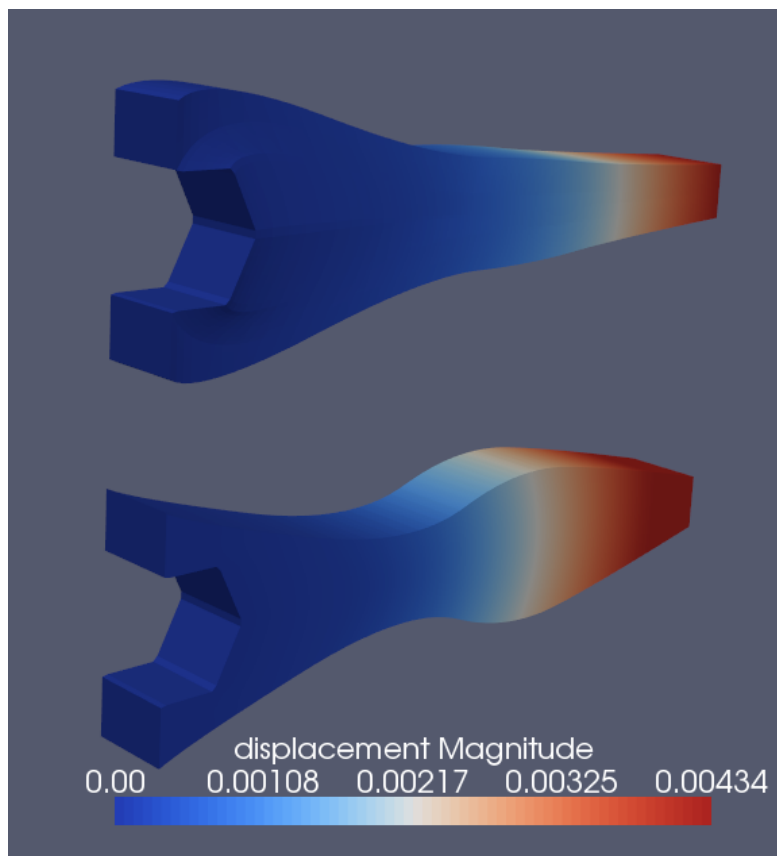Figure 15: Comparison of the initial (white) and final (blue) domains for the first exercise.

Figure 16: Comparison of the initial (bottom) and final (top) displacement fields for the first exercise.
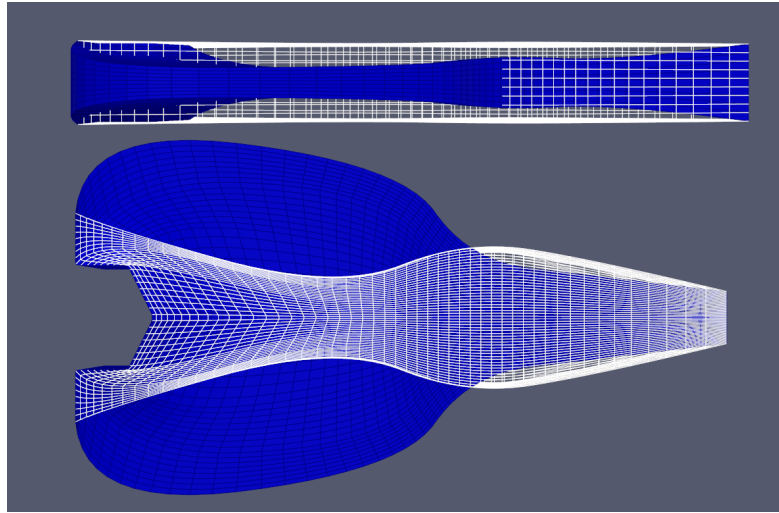
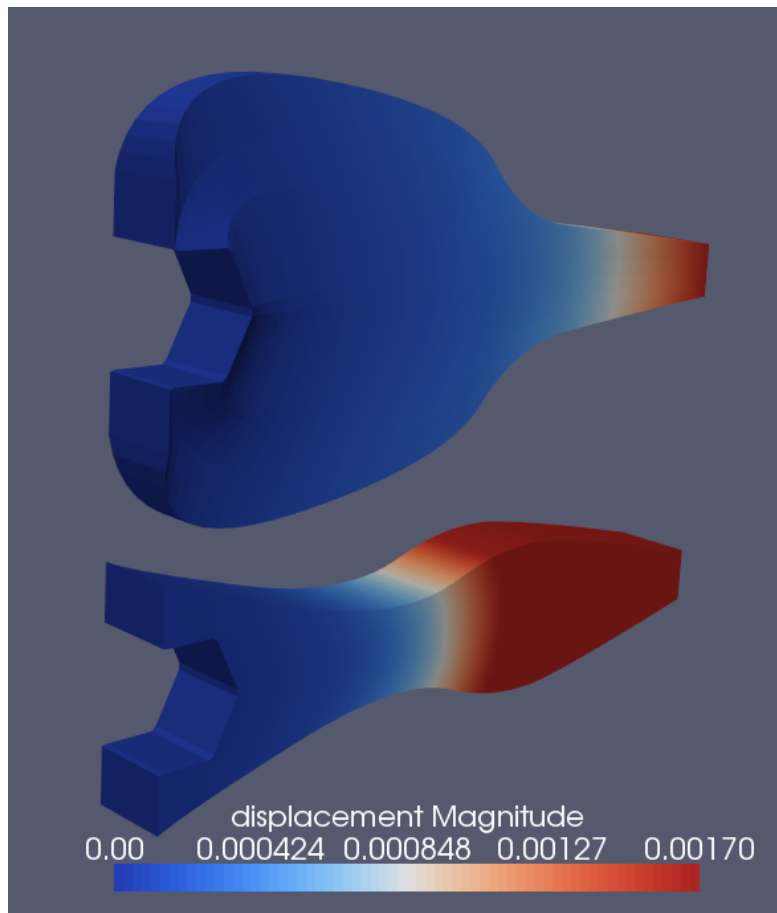Figure 17: Comparison of the initial (white) and final (blue) domains for the second exercise.

Figure 18: Comparison of the initial (bottom) and final (top) displacement fields for the second exercise.

9   Conclusion

This study has demonstrated that isogeometric analysis provides an attractive theoretical and practical framework for sensitivity analysis and shape derivative computation. The concept of shape derivatives has been set-up in this context for linear elasticity problems and used for practical shape optimization exercises.

The main ingredient is the use of the same NURBS representation for the computational domain, the structural displacement field, the shape gradient on the moving boundary and the domain deformation during the design process. The uniqueness of the geometrical representation makes the implementation straightforward and avoids the introduction of spurious errors in the design optimization loop.

Nevertheless, several improvements are still required to face industrial problems: from a practical point of view, the approach needs to be extended to multi-patch representations, to describe more complex geometries, and local refinement techniques should be introduced to improve computational efficiency. From a methodological point of view, more complex problems should be considered in the future, for instance exhibiting non-linear behavior.

Acknowledgements

References

[1] G. Allaire, F. Jouve, and A.M. Toader. Structural optimization using shape sensitivity analysis and a level-set method. *J. Comput. Physics*, 194, 2004.

[2] Y. Bazilevs, L. Beirão da Veiga, J. A. Cottrell, T. J. R. Hughes, and G. Sangalli. Isogeometric analysis: Approximation, stability and error estimates for h-refined meshes. *Mathematical Methods and Models in Applied Sciences*, 16:1031–1090, 2006.

[3] J.A. Cottrell, T.J.R. Hughes, and Y. Bazilevs. *Isogeometric analysis : towards integration of CAD and FEA*. John Wiley & sons, 2009.

[4] J.A. Cottrell, T.J.R. Hughes, and A. Reali. Studies of refinement and continuity in isogeometric analysis. *Computer Methods in Applied Mechanics and Engineering*, (196):4160–4183, 2007.

[5] T. A. Davis and I. S. Duff. A combined unifrontal/multifrontal method for unsymmetric sparse matrices. *ACM Transactions on Mathematical Software*, 25(1), 1999.

[6] C. De Boor. *A Practical Guide to Splines*. Springer Verlag, 1978.

[7] M. Delfour and J.-P. Zolesio. *Shapes and geometries: analysis, differential calculus, and optimization*. SIAM, 2001.

[8] M. Dorfel, B. Juttler, and B. Simeon. Adaptive isogeometric analysis by local h-refinement with t-splines. *Computer Methods in Applied Mechanics and Engineering*, 199(5-8), 2010.

[9] G. Farin. *Curves and Surfaces for Computer-Aided Geometric Design*. Academic Press, 1989.

[10] J. Hadamard. Mémoire sur le problème d'analyse relatif à l'équilibre des plaques élastiques. *Bulletin de la Société des Mathématiques Françaises*, 1907.

[11] T.J.R. Hughes, J.A. Cottrell, and Y. Bazilevs. Isogeometric analysis: Cad, finite elements, nurbs, exact geometry, and mesh refinement. *Computer Methods in Applied Mechanics and Engineering*, (194):4135–4195, 2005.

[12] E. Nielsen and M. Park. Using an adjoint approach to eliminate mesh sensitivities in computational design. In *43th AIAA Aerospace Sciences Meeting and Exhibit*, 2005.

[13] O. Pironneau. *Optimal shape design for elliptic systems*. Springer-Verlag, 2983.

[14] X. Qian. Full analytical sensitivities in NURBS based isogeometric shape optimization. *Computer Methods in Applied Mechanics and Engineering*, 199(29-32), 2010.

[15] M. Sabin. Cad system components. *Computer Aided Design*, 25(3):119–140, 1993.

[16] Y.-D. Seo, H.-J. Kim, and S.-K. Youn. Isogeometric topology optimization using trimmed spline surfaces. *Computer Method in Applied Mechanics and Engineering*, 199(49-52), 2010.

[17] J. Sokolowski and J.-P. Zolésio. *Introduction to shape optimization*. Springer Verlag, 1992.

[18] A.V. Vuong, C. Giannelli, B. Juttler, and B. Simeon. A hierarchical approach to adaptive local refinement in isogeometric analysis. *Computer Method in Applied Mechanics and Engineering*, 200(49-52), 2011.

[19] Wolfgang A. Wall, Moritz A. Frenzel, and Christian Cyron. Isogeometric structural shape optimization. *Computer Methods in Applied Mechanics and Engineering*, 197(33-40):2976–2988, 2008.

Contents